Published in final edited form as:
Inorganica Chim Acta. 2012 December 1; 393: 12–23. doi:10.1016/j.ica.2012.06.026.

Imaging free zinc levels *in vivo* - what can be learned?

Luis De Leon-Rodriguez[1], **Angelo Josue M. Lubag Jr.**[2], and **A. Dean Sherry**[2,3]

[1]Departamento de Quimica. Universidad de Guanajuato. Cerro de la Venada S.N. Col. Pueblito de Rocha., Guanajuato, Gto. Mexico, C.P, 36040

[2]Advanced Imaging Research Center and Department of Radiology, University of Texas Southwestern Medical Center at Dallas, 5323 Harry Hines Blvd., Dallas, TX 75390-8568

[3]Department of Chemistry, University of Texas at Dallas, 800 West Campbell Rd., Richardson, TX 75083-3021

Abstract

Our ever-expanding knowledge about the role of zinc in biology includes its role in redox modulation, immune response, neurotransmission, reproduction, diabetes, cancer, and Alzheimers disease is galvanizing interest in detecting and monitoring the various forms of Zn(II) in biological systems. This paper reviews reported strategies for detecting and tracking of labile or “free” unchelated Zn(II) in tissues. While different bound structural forms of Zn(II) have been identified and studied *in vitro* by multiple techniques, very few molecular imaging methods have successfully tracked the ion *in vivo*. A number of MRI and optical strategies have now been reported for detection of free Zn(II) in cells and tissues but only a few have been applied successfully *in vivo*. A recent report of a MRI sensor for *in vivo* tracking of Zn(II) released from pancreatic β-cells during insulin secretion exemplifies the promise of rational design of new Zn(II) sensors for tracking this biologically important ion *in vivo*. Such studies promise to provide new insights into zinc trafficking *in vivo* and the critical role of this ion in many human diseases.

Keywords

Tissue zinc levels; imaging free zinc; zinc homeostasis; MRI

1. Introduction

Divalent zinc (Zn(II)) is a constituent of about 3,000 human proteins and required for over 300 cellular processes from DNA transcription to protein synthesis, assisting in enzyme structural and catalytic activity, neurotransmission, intracellular signaling, and antibiotic activities [1–3]. It has relatively limited bioavailability with a total mass in an adult human estimated at between 2–4 g [4], second only to iron from the d-block metals. The amount of Zn(II) in blood is maintained at a very tight and low concentration range of 12–16 μM [4, 5] mostly in chelated, protein-bound Zn(II) forms [5, 6]. However, some cells of the pancreas [7], prostate [2, 3, 8], breast [9], brain [2, 10–13] and gastro-intestinal tract [14, 15] are known to have local concentrations of Zn(II) as high as several mM. Insulin is packaged

Address all correspondence to this author at dean.sherry@utsouthwestern.edu. Telephone: 972-645-2730 Fax: 214-645-2744.

with Zn(II) in secretory granules in β-cells and the local concentration of Zn(II) in those granules has been estimated to be as high as 10–20 mM [16]. The specialized epithelial cells in the normal peripheral zone of the prostate gland contains between 3,000 to 4,500 nmol/g wet tissue weight (~ 3 – 4.5 mM) while the normal prostatic fluid as much as 10,000 nmol/g (~ 10 mM) [8] and a total Zn(II) ~ 2.5 mM when averaged for the whole prostate [3]. The mammary cells are expected to produce about 1 – 3 μg Zn/d during lactation to meet the needs of the developing infant and are known to hyper-accumulate Zn(II) in malignant breast tumors [3] (See Table 1). Thus, it is clear that Zn(II) plays a pivotal role in the biology and physiology of some cell types more than others.

One of the most profound functions of Zn(II) in living systems is its unequivocal role in oxidative balance. The redox state of a cell or cell compartments has been shown to correlate with the redox state and abundance of Zn(II)-binding carrier metallothioneins (MTs) in cells or particular cell organelles [17–20]. Studies indicate that the ratio of thionein (i.e., the MT without Zn) to metallothionein (T/MT) control Zn(II) availability and the activity of some enzymes [21]. Mammalian MTs can structurally carry as many as 7 Zn(II) ions per molecule and binding occurs via a sequential, non-cooperative mechanism [22–24]. These MTs have been classified into three groups: tight, moderate, and loose binders based on affinity and availability of the Zn(II) binding sites. The tight binding sites for Zn(II) (log K > 11) involve the first four thiol groups in cysteines of the MTs while moderate binders (log K between 9 and 11) and loose binding have log K values ~ 7.7 [21, 22, 25–28]. These forms are known to participate in a wide variety of redox reactions and Zn(II) transport in cells and specific organelles through reactions with other known redox active species such as glutathione [24] and NO [29]. As changes in the amount of free unbound Zn(II) is known to trigger a multitude of genes, dysfunctions involving MTs in mammals are thought to ultimately pave the way for greater oxidative stress and possibly cancer [30], a better understanding of both how much and which forms of zinc are involved *in vivo* are warranted.

The different forms of Zn(II) depends on the multiple compartments, ligands, and interactions *in vivo* – i.e., with transporters (e.g., ZIP and ZnT families) [31–34], carrier proteins (e.g., metallothioneins, albumins) and small molecules (e.g., phosphates/ phosphonates) [35], or by exocytosis through secretory granules. Specialized cells in the specific organs have been shown to store Zn(II) in MTs, release Zn(II) (e.g., exocytose free Zn) and pump the ion across cell membranes *via* transporters. These events occur in response to certain biochemical triggers such as hormone release or changes in nutrient level as part of normal biological rhythms or cell cycles. Extreme conditions and morbidities that correlate with abnormal Zn(II) local levels are of high biological significance; Zn(II) deficiency and/or elevated levels have been known to be linked with oxidative stress/ protection [36, 37] and also oxidative defense/damage to lipids, proteins and nucleic acids that correlate with numerous ailments [36, 38–41]. Another example is the long established release of Zn(II)-insulin granules from β-cells in response to elevated blood glucose (e.g., post-prandial). Changes in the total mass and the functional activity of β-cells have been adopted as indexes of diabetes [42, 43]. Free Zn(II) is known to be co-released with insulin in well-defined proportions in healthy individuals [40, 44] but there are other specialized cells known to have such Zn(II)-rich secretory granules as well (see Table 1). These all have the potential to elevate extracellular free Zn(II) upon stimulation. However, it is not known exactly how abnormal (chronic or acute), local (cellular or sub-cellular), or regional (tissue or organ) Zn(II) release or concentration changes, can cause (or be actual outcomes of) certain disease states, e.g., diabetes, prostate cancer or breast cancer. In view of the need to study and track Zn(II) homeostasis and correlate variations in Zn(II) levels with disease, techniques that might allow monitoring of free Zn(II) ions and their localization *in vivo* remains an unmet need.

The 'activity' of free Zn(II) in biology is often quantified as −log [Zn(II)] or pZn. Here, pZn refers to the activity or concentration of "rapidly exchangeable" or free Zn(II) in a particular tissue. Frederickson et al. (2006) estimated that pZn ≈ 7.7 (equivalent to 19 nM free ion; 95% range: 5–25 nM) in extracellular cerebral spinal fluid of rat, rabbit and humans [45]. This value was claimed to be three orders of magnitude lower than previous estimates of the physiological concentration of free Zn(II) necessary to stimulate neuronal tissue. This does not mean that the total concentration of the ion, i.e., including all forms, is ~20 nM. The majority of biological Zn(II) is most cell types (with the exception of certain cells containing Zn in secretory vesicles) is quite low as estimated by using commonly available immune-staining techniques or chelating type dyes, e.g., dithizone, typically used for Zn(II) staining. It is estimated that, although local synaptic events release free Zn(II) at micromolar levels locally, the non-event levels are in the picomolar range [46]. Even though detection methods, function, activity, and homeostasis of Zn(II) have been the subject of a very rapidly growing area of research in the past decade, there is still a relatively limited body of knowledge about Zn(II) levels, transport dynamics (i.e., biochemistry and flux), and control compared to other well-studied biologically active ions such as calcium. This review focuses on the literature relevant to tracking and imaging the biologically relevant form of reactive zinc, free Zn(II), using appropriate molecular probes and imaging technologies.

2. Technologies for imaging free Zn(II) in vivo

Imaging has become an indispensable tool in research, clinical trials and medical practice. Recently, there has been an increased interest on the applications of imaging technologies aiming to visualize the expression and activity of particular molecules, cells and biological processes that influence growth of abnormal tissues and/or responsiveness to therapeutic drugs. Imaging techniques that have no limitation on the depth of the sample to be examined are particularly important for monitoring molecular events in human subjects. Magnetic resonance imaging (MRI) and nuclear imaging techniques such as PET or SPECT fulfill this requirement while most optical techniques are limited to cells in culture, tissues near the skin surface or *in vivo* surface analysis [47]. Direct readout of free Zn(II) in living subjects is impossible with any standard imaging technique available today so the use of zinc specific molecular sensors is required. For the most part, sensors in the form of small molecules that fluoresce upon binding with Zn(II) have been most widely studied for imaging labile zinc ions in cells and tissues using optical techniques. Comprehensive reviews of fluorescent zinc sensors can be found in the literature [48–50]. The present survey will focus on those sensors that have either been applied in whole animal studies or have the potential to do so.

2.1 Magnetic resonance imaging (MRI)

MRI offers high spatial resolution but poor sensitivity compared to nuclear imaging or optical techniques. Most MRI molecular sensors are based on paramagnetic metal ion complexes (mainly Gd(III) or Mn(II)) that shorten the longitudinal relaxation times (T_1) of protons of water molecules of those tissues where the sensor is distributed. Such agents, referred to as T_1 contrast agents (CA), are widely used to identify leaky tissues such as tumors growing in brain or to characterize tissue perfusion or vascularity by imaging the dynamics of CA passage through the tissue. The efficiency of a CA is measured in terms of T_1 relaxivity (r_1) which reflects the ability of an agent to decrease the T_1 of the water protons per unit concentration (mM) concentration of agent. T_1 agents designed to detect Zn(II) typically rely upon a change in r_1 (preferably a large change) that occurs upon binding of Zn(II) to an agent. Ideally, the agent would be 'off' in the absence of Zn(II) and 'on' when bound to Zn(II). Usually, an increase in r_1 is considered optimal because this translates into image contrast enhancement or brightening when Zn(II) is present in sufficient quantity to saturate the agent binding domain. In practice, agents of this type are never completely off at typical doses so this adds the additional complexity of trying to

differentiate between a Zn(II) binding event *versus* a higher concentration of agent. In practice, r_1 can be modulated by either by changing the number of water molecules coordinated to the paramagnetic center (q), by altering the rate of water exchange (τ_M), or by slowing the molecular tumbling time of the sensor (τ_R). The earlier literature on Zn(II) selective MR agents can be found in two recent reviews [51, 52] while other designs have appeared since those reviews were published [53–56]. MRI-based sensors are typically composed of a paramagnetic metal ion, a ligand to encapsulate the paramagnetic ion, and a Zn(II) binding selective chelating unit (Fig. 1). 1,4,7,10-tetraazacyclododecane-1,4,7,10-tetracetic acid (DOTA) has been the preferred ligand for Gd(III) for many years, largely due to the favorable thermodynamic and kinetic stability of these complexes while di-2-picolylamine (DPA) has been the most popular receptor for constructing the Zn(II) binding domain [57]. DPA displays high selectivity for Zn(II) over alkali and alkaline-earth metal ions that occur in much higher concentrations in biological systems (Ca^{2+}, Mg^{2+}, K^+ and Na^+) but little to no selectivity over divalent ions of similar size and coordination chemistry (i.e., Cu^{2+}). Diacetateamine (daa) is another chelating moiety often used for Zn(II).

Several MRI agents that respond to Zn(II) binding by showing an increase in r_1 as a result of an increase in q from zero to one have been reported [54, 58, 59]. The first of these, Gd-daa3 (Fig.1), displayed a 121% increase in r_1 upon addition of Zn(II) in aqueous buffer (Table 1) but only a modest 33% increase in r_1 when measured in human serum [58]. A second generation agent, Gd-apa3 (Fig.1) with a picolyl group substituted for one acetate [59], displayed a 102% increase in r_1 upon addition of Zn(II). Further substitution of the remaining acetate with a second picolyl group resulted in an agent that binds Zn(II) while r_1 remained unchanged. This confirmed the necessity of having at least one acetate group for successfully blocking water access to the GdDO3A moiety. More recently, a somewhat different approach was used to block water access to Gd(III) by using an amide carbonyl group on the fourth arm of GdDO3A (Gd-L^1, Fig. 1). Interestingly, in this model, the amide carbonyl group binds to Gd(III) in the absence of Zn(II) but then switches its binding allegiance to Zn(II) when the divalent ion is attracted to the tridentate daa binding unit [54]. A 70% increase in r_1 was observed during this binding event in buffer but, again, only a more modest 40% increase in r_1 in mouse serum (Table 1). One interesting feature of this agent was that Gd-L^1 also binds Cu(II), but in this case, r_1 was not significantly altered upon binding. While the applications of these zinc-activated MRI probes have been postulated for imaging Zn(II) in the extracellular fluids of the brain where Zn(II) can presumably reach up to 200–300 μM following stress-induced release from neuronal synaptic vesicles, *in vivo* applications of these agents have not been reported.

The paramagnetic properties of divalent manganese (d^5) are also reasonably favorable for T_1 contrast enhancement applications and this ion has the added benefit of being naturally present at low levels in mammalian tissues. For this reason, Mn(II) complexes are generally considered less toxic than complexes of Gd(III) (assuming the toxicity arises from release of the free ion *in vivo*). Recently, a rather interesting Mn(III)-porphyrin-derivative was reported as a MRI sensor of Zn(II). Mn-(DPA-C_2)$_2$-$TPPS_3$ (Fig. 1) is interesting because it appears to be more permeable to cell membranes, a feature lacking in most Gd(III)-based agents. An unexpected finding was that the r_1 of this agent decreases from 8.7 to 6.6 $mM^{-1}s^{-1}$ upon exposure to Zn(II) in buffer (Table 1), so instead detecting the presence of Zn(II) as in increase in image intensity, one would expect to find darkening of the image when the agent binds to Zn(II). Somewhat surprisingly, however, this was not observed when the agent was added to HEK-293 cells; rather, greater contrast enhancement (shorter T_1) was seen when the agent was incubated with cells in presence of exogenous Zn(II) than when incubated with cells in the absence of Zn(II) [60]. This feature can only be attributed to greater cell uptake for the neutral or positively charged ternary Mn-(DPA-Zn_n-C_2)$_2$-$TPPS_3$ (n= 1 or 2) complexes compared to the negatively charged, zinc-free probe. *In vivo*

detection of this agent was also demonstrated by direct injection of two different agents (Mn-(DPA-C_2)$_2$-TPPS$_3$ and Mn-TPPS$_4$ as a control) into different tissue regions of rat brain [61]. Two days after injection, T_1-weighted images of brain showed an increase in contrast in the hippocampus (HP) and the caudate-putamen (CP) for the Zn(II) binding agent compared to the control agent (see Figs 2A and 2B), again consistent with greater cell uptake of Mn-(DPA-C_2)$_2$-TPPS$_3$ in those tissue regions known to have more labile Zn(II) (the HP). Thus, even though the T_1 characteristics of this agent are not considered terribly favorable for detecting Zn(II) based solely on changes in relaxivity, this agent is unique in that it appears to concentrate in cells that contain more Zn(II) (analyte-dependent transport). This feature may ultimately prove to be even more favorable for imaging Zn(II) *in vivo* compared to those that respond by showing large changes in T_1 or T_2 relaxivity. Porphyrin derivatives such as this may also prove to be more easily modified to enable them to cross the blood-brain barrier. This will ultimately be necessary to monitor regions of brain with abnormal levels of Zn(II) in a non-invasive fashion by MRI. Finally, another nice feature of Mn-(DPA-Zn_n-C_2)$_2$-TPPS$_3$ is that also can act as an optical sensor for Zn(II) [60].

Inspired by the first report of a Zn(II)-sensitive MRI contrast agent, a GdDTPA-derivative containing two DPA binding moieties [62], we set out to design a structure based on the more stable GdDOTA framework (GdDOTA-diBPEN, Fig. 1). While the macrocyclic sensor showed only a modest 20% increase in r_1 upon addition of 2 equivalents of Zn(II) in buffered media, it showed a surprising 164% increase in r_1 in buffered media containing fatty acid free human serum albumin (HSA) (Table 1). This feature was traced to a slowing of molecular rotation (τ_R) upon binding of GdDOTA-diBPEN-$(Zn)_2$ to site 2 of HSA with a K_D ~ 40 μM [63]. A more modest increase in r_1 of 40% was observed for the agent in serum suggesting that other components in the serum may compete for the agent binding site on HSA. The higher r_1 value of GdDOTA-diBPEN compared to clinical extracellular agents (eg. Prohance™, Table 1) plus the enhancement in r_1 that occurs upon Zn(II) binding suggested to us that GdDOTA-diBPEN might be sensitive enough for use *in vivo* at doses much lower than those used for clinically approved agents (0.1 mmol/Kg). It would be particularly useful if a responsive agent such as this could be administered at a level where it is essentially silent in the absence of Zn(II) (based on a low tissue concentration) but then becomes detectable only when Zn(II) is bound. To test this concept *in vivo*, we chose the pancreas as our first target [64]. It is known that Zn(II) ions are required for proper storage of insulin granules in β-cells (~2:1, Zn(II):insulin) and that Zn(II) is released from β-cells during exocytosis of insulin. The released Zn(II) ions are thought to bind weakly to extracellular matrix proteins, including perhaps MTs, in the immediate vicinity of β-cells and therefore should be available for competitive binding to GdDOTA-diBPEN [65]. It had been predicted that the release of insulin from granules elevates Zn(II) in the immediate vicinity of β-cells to the 400–500 μM range [66], clearly high enough to fully saturate the binding sites on GdDOTA-diBPEN. To test this, 24 hour fasted mice were injected (*i.p.*) with a bolus of glucose (to yield a blood glucose concentration of ~17 mM) to initiate insulin secretion. Ten minutes later, GdDOTA-diBPEN at a dose of ~0.03 mmol/Kg was injected *i.v.* This dose corresponds to an extracellular concentration of ~50 μM, about 3–4 fold lower than the typical clinical dose of a typical extracellular Gd(III)-based contrast agent. Fifty micromolar was determined empirically to be the optimal concentration to meet the requirement of little to no MR detection of the agent in the absence of Zn(II) but a substantial shortening of T_1 to yield clear MR signal enhancement when the GdDOTA-diBPEN-$(Zn)_2$ complex forms and binds to albumin [64]. Using this protocol, functional release of Zn(II) from the pancreas of mice was readily detected during glucose stimulated insulin secretion (GSIS) from β-cells. In subsequent experiments, another group of mice were fed a high fat diet over a period of 12 weeks. These animals became hyperinsulinemic due to skeletal muscle insulin resistance and, in response, the pancreas expanded to meet the increased demand for insulin. This increase in β-cell mass (the insulin producing cells) was

easily detected by MRI using this Zn(II) sensor (Fig. 3). Finally, to illustrate that GdDOTA-diBPEN would not respond in the animals lacking functional β-cells, a condition typical of type 1 diabetics, a separate group of mice were pretreated with the β-cell toxin, streptozotocin (STZ), and then imaged (Fig. 4). As anticipated, the pancreas was not enhanced by the agent following a bolus of glucose in those animals, consistent with complete loss of β-cell function and consequently no release of Zn(II).

The images shown in Figures 3 and 4 illustrate that Zn(II) release from β-cells is easily detected *in vivo* by MRI. This has been used to show that β-cell function increases with age and growing insulin resistance that accompanies accumulation of fat in tissues, including the pancreas. Although the images shown in Figure 3 reflect only a single slice through the pancreas, collection of fourteen adjacent slices through the abdomen (collected over 2 min) provided a 3D view of the functional pancreas and allowed a measure of the "functional volume" as reflected by Zn(II) release (shown as the color overlay). Although β-cell mass was not measured in this study, the "functional volume" as measured by MRI was 34 mm^3 at 12 weeks of age, 44 mm^3 at 24 weeks on a normal diet, and 58 mm^3 after 12 weeks on a control diet plus 12 weeks on a high fat diet. These volumes represent a volume of tissue that is ~18-fold larger than the volume (or mass) of β-cells as measured by independent methods [67]. This larger functional volume is consistent with diffusion of Zn(II) ions away from β-cells after their release into the extracellular medium. This study raises a number of interesting questions concerning the role of Zn(II) ions released from β-cells. What does diffusion of Zn(II) excreted from β-cells into the surrounding tissue spaces tell us? Is Zn(II) functioning as a signaling ion between different types of cells in the pancreas? Does GdDOTA-diBPEN bind with Zn(II) so strongly that it interferes with "normal" β-cell physiology? Can the MRI signal of this agent be used to quantify the total amount of Zn(II) released from β-cells? While further studies will be required to answer these questions, the use of GdDOTA-diBPEN as a MRI sensor of Zn(II) appears to be a promising tool that may help reveal some of the mysteries of the role of free Zn(II) *in vivo*.

A second generation DOTA-based Zn(II) sensor where the DPA units were substituted by 3-methylpyrazolyl (BPYREN) groups was reported more recently (GdDOTA-diBPYREN, Fig. 1)[55]. The 3-pyrazolyl moiety was chosen because it retains a pyridine-like nitrogen atom (N^2) to act as a donor atom for Zn(II) but also has a neighboring N^1H group known to stabilize metal ion complexes via added hydrogen bonding interactions, a feature that could strengthen the binding interaction between the Zn(II)-agent and HSA. GdDOTA-diBPYREN displayed a 64% increase in r_1 when Zn(II) was present in buffer and showed an impressive 118% increase in r_1 when placed in human serum, the largest change reported for a Zn(II) agent in this type in a biological medium. This behavior was attributed to a slightly improved affinity for GdDOTA-diBPYREN-$(Zn)_2$ on the binding site of HSA (K_D ~ 29 μM) compared to that seen earlier for GdDOTA-diBPYREN-$(Zn)_2$ (42 μM). Despite the fact that the BPYREN group showed a much weaker binding affinity for Zn(II) (K_D ~ 378 μM) when compared to BPEN (K_D ~ 33 nM) (attributed to the strong electron-withdrawing effect of N^1), a contrast enhancement in the duodenal region of the pancreas was observed in mice during GSIS when the GdDOTA-diBPYREN was administered at a typical clinical dose (0.1 mmol/Kg). This finding indicates that the local Zn(II) concentration in the vicinity of β-cells must be in the high μM range.

2.1.1 Optimizing Zn(II) selective sensors for MRI—The usual goal in the design of Zn(II) sensors for MRI is a large increase in relaxivity (either r_1 or r_2 but most often r_1), but there are other factors to consider. Among them includes questions such as what is the biological target, what is the optimal Zn(II) binding affinity for that target, and what degree of metal ion selectivity is required?

2.1.1.1 Biological Targets: One of the main limitations of MRI as a tool for molecular imaging is the low sensitivity of NMR compared to optical or nuclear imaging methods. The detection limit (DL) of typical clinical MRI contrast agents is between 50 and 500 μM depending upon the relaxivity of the agent. For responsive agents, the DL is determined by the concentration of the targeted metabolite or ion and by Δr_1, the change in r_1 observed upon metabolite or ion recognition. Biological targets that have free chelatable or weakly bound Zn(II) on the order of ~1 μM would require a sensor that reaches $r_1 \sim 100\ mM^{-1}s^{-1}$ upon Zn(II) binding [68]. Even though a T_1 relaxivity as high as this can be reached by attaching several agents to a multimeric scaffold [69], this relatively high DL dismisses the possibility of monitoring free Zn(II) by MRI in the nM range, a level typical of most cells or organs. Based on these estimates, it is reasonable to conclude that one should consider biological targets for MRI where labile Zn(II) is found at 1 μM or higher. It has been reported that brain, pancreas and prostate contain high levels of Zn(II), but most importantly, high labile Zn(II) concentrations are present in these organs or can be reached under certain physiological conditions. It has been postulated that concentrations of labile Zn(II) in cerebrospinal fluid may rise from 10 nM to values as high as 300 μM following stress-induced release of Zn(II) from neuronal synaptic vesicles [70]. It is also known that β-cells release labile Zn(II) simultaneously with release of insulin such that the local concentration of Zn(II) surrounding activated β-cells may be as high as 480 μM [66], ~20x higher than the total Zn(II) concentration in blood. The levels of Zn(II) in prostate are the highest among all the soft organs; for example, the normal peripherial zone has a total Zn(II) concentration of ~3 mM while prostatic fluid has Zn(II) levels of ~9 mM. In adenocarcinoma, total Zn(II) in these same regions drop to ~0.4 and ~0.8 mM, respectively [71]. The peripheral zone which consists of highly specialized glandular secretory epithelial cells comprises about 70% of the prostate and is responsible for Zn(II) accumulation. It is known that labile Zn(II) in the cytosol of prostate epithelial cells can be as high as 300 μ [72]. Imbalances of labile Zn(II) in brain, pancreas and prostate are related to pathologies such as neurodegenerative disorders (e.g. Alzheimers) [73], diabetes [74] and prostate cancer [71] so one must consider the inherent difficulties of measuring Zn(II) over a wide range of concentrations when designing a Zn(II) sensor for MRI. While the pancreas and prostate are relatively easy to target because they have full access to the blood, reaching the brain with a MRI agent is particularly difficult because of the brain blood barrier (BBB). The BBB is a lipophilic endothelial interface which limits passive uptake of hydrophilic, ionic and large molecules between blood and the extracellular fluid of brain parenchyma. All MRI-responsive Zn(II) sensors reported to date are hydrophilic and/or ionic (Fig. 1) and therefore most likely will not cross the BBB. Although there are several known strategies used to enhance the uptake of molecules into brain, the design of agents attached to vectors that could nondestructively penetrate the BBB seems to be the most suitable approach given the polar nature of most MRI CA [75, 76]. This makes derivatives of the Mn-porphyrin system described above attractive for imaging abnormal levels of Zn(II) in the brain.

2.1.1.2 Zn(II)binding affinity: Once that the potential target organ of interest is identified, the binding constant (K_{DZnCA}) of the agent for the levels of Zn(II) found in that tissue must be considered. The simplest predictive model consists of calculating the relaxation rate change (ΔR_1, where $R = 1/T_1$) expected at equilibrium for a given concentration of agent and Zn(II) when passing from a basal Zn(II) level to an altered physiological state. The data shown above for stimulation of Zn(II) release from the pancreas by added glucose is a good example. A more realistic model, however, should consider the binding competition of Zn(II) between the sensor and all other natural Zn(II) chelators. One additional constraint should be for the sensor not to have a significantly higher binding affinity for Zn(II) than any essential enzyme or protein, because this could result in an imbalance of free Zn(II) levels, especially when given the high concentration of agent required for MRI contrast.

Thus, a K_D in the tenths of nM or higher might be a reasonable target for any new sensor design. One also needs to consider how high the K_D of a Zn(II) sensor could be while remaining useful for detection of the metal *in vivo*. One could argue that this is best determined by experimentation, but a reasonable estimate can be found if one considers the *in vivo* mechanisms that help to maintain Zn(II) homeostasis during high extracellular secretion of Zn(II). As discussed in the introduction, it is known that several transporters participate in the extracellular uptake of free Zn(II) (zinc-importing proteins; e.g. ZIP1 [72], and zinc-transporters; e.g. ZT1, ZT3, ZT8 [77] and voltage-gated calcium channels [65]). Moreover, it is also know that Zn(II)-buffering proteins or small ligands (e.g. amino acids) can bind free Zn(II) and assist in cell uptake of the ion, an important consideration given the cytotoxicity of free Zn(II) at high concentrations [78]. Some buffering proteins include HSA (K_{DZnHSA} = 29.5 nM) [79] and metallothioneins (MTs). MTs can bind up to seven Zn(II) ions with one Zn(II) ion being relatively weakly bound (K_{DZn7MT}= 19.9 nM) [80], and therefore considered labile compared to enzymes and many proteins. Thus, a natural Zn(II) chelator with a K_{DZn} between 10 and 30 nM would compete for Zn(II) from these more loosely bound sites. If one considers that HSA is found at higher concentrations than MTs in extracellular fluids (HSA is 600 μM in blood while MT is 0.5 nM) [81], then one can set up a simple competitive binding model to estimate a target binding constant for a Zn(II) sensor (K_{DZnCA}) that would compete effectively with HSA for free Zn(II) and the ΔR_1 needed for detection as free Zn(II) increases from some basal level of ~20 μM (total Zn(II) in blood) to an abnormal physiological state (such as 480 μM Zn(II) near β-cells during insulin release). If one assumes an r_1 of 4.0 $mM^{-1}s^{-1}$ for an unbound CA and 5.6 $mM^{-1}s^{-1}$ for the Zn(II) bound CA (a ~40% change is the average relaxivity change reported for Zn(II) sensors, Table 1), then one could generate the curves shown in Fig. 5 for different values of K_{DZnCA}.

If one assumes $\Delta R_1 \sim 0.07$ is the lower detection limit [82], then one would conclude that only Zn(II) sensors having a $K_{DZnCA} < 1$ μM would be able to detect 480 μM free Zn(II) by MRI. While this model predicts the success of GdDOTA-diBPEN in detecting release of free Zn(II) from pancreatic β-cells [62], the same model may not necessarily work for all tissues and other physiological conditions. For example, the extracellular concentration of HSA in brain is ~ 3 μM [83] while basal levels of Zn(II) are ~10 nM, so if one assumes that an agent concentration of 50 μM could be reached in brain tissue, then one would predict that a Zn(II) sensor with a K_{DZnCA} of 10 μM would detect free Zn(II) levels of ~100 μM or higher. It is also compelling to consider that under these conditions a Zn(II) MRI CA might also serve as a theragnostic agent for Alzheimer's disease by removing Zn(II) from β-amyloid plaques ($K_{DZn\text{-}A\beta40} \sim 2$ μM) [84]. Fig. 6 summarizes K_{DZn} values for important biological proteins and ligands such as the Zn(II) MRI CAs reported herein. Labile Zn(II) concentrations in different organs are also included so that this figure can serve as a general guide when designing new Zn(II) probes. From Fig. 6, it becomes evident that the K_{DZn} of any new CA should be no lower than the K_{DZn} of enzymes or structural proteins and no higher than the concentration of labile Zn(II) for a particular target. If one considers that the lower concentration limit of labile Zn(II) for a particular region could be estimated when administering the CA at a dose where it is "off" in absence of Zn(II) but "on" when labile Zn(II) reaches a specific threshold [63], then the importance of having a toolbox of Zn(II) MRI CAs with binding constants that cover a wide range of K_{DZnCA} values becomes quite evident.

The K_{DZnCA} values of currently known CAs cluster in two main regions (see panel B of Fig. 6) so it is clear that such a toolbox does not yet exist. Much can be learned about the design of Zn(II) MRI CAs with appropriate K_{DZnCA} values by surveying the extensive literature on fluorescent Zn(II) probes where several variants of the DPA chelator have been reported (Fig. 7). The inclusion of a methyl group in position 6 of the picolyl units decreases K_{DZn} due to steric hindrance (see entries **8**, **9**, **21** and **22** in Fig. 7). Substitution of one picolyl unit

by a non-coordinating moiety has a dramatic detriment effect on K_{DZn} (see entries **10**, **12**, **14** and **24**). A less dramatic but similar trend is observed when the picolyl unit is either substituted by another electron rich or softer coordinating unit (see entries **15** and **18**) or when an electron withdrawing atom is present in the pyridine ring (see entry **11**). An important increase in K_{DZn} is seen when the 2-methylpyridyl group is changed by a 2-ethylpyridyl (see entries **25** and **26**), which might be attributed to geometric constraints impose by lengthening the alkyl chain. Surprisingly an important weakening Zn(II) binding effect is observed when the hydrophobicity of the whole molecule is altered (see entries **21** and **27**). Given these known relationships between K_{DZn} and the chemical structure of the Zn(II) binding unit, it is clear that similar approaches could be used to design a series of new Zn(II) MRI CAs.

If one wants to design a CA that does not interfere or participate in a biological process involving Zn(II) then not only the thermodynamic stability of the Zn(II) agent should be considered but also the kinetic stability constants. It is known that certain chelating agents can accelerate removal of Zn(II) from enzymes by initially forming a ternary complex. The term “catalytic chelation” was introduced to describe a mechanism where a chelating agent binds to the Zn(II)-enzyme, aids in decomplexation of Zn(II) from the enzyme and then transfers the ion to a second chelating agent with potentially higher affinity but lacking the capacity to interact directly with Zn(II) in its binding site on the enzyme [86]. A better understanding of the relationship between thermodynamic stability and kinetic lability can be seen if one looks into Zn(II) self-exchange rates. For instance it is known that “radiozinc (^{65}Zn) exchanges with Zn(II) in proteins” (e.g. carbonic anhydrase II, superoxide dismutase) on the order of days or longer. However, self-exchange rates in mammalian metallothionein, where direct molecular contact is possible, occurs on the order of minutes. It has also been shown that small ligands can accelerate the rate of Zn(II) ion exchange up to 420-fold [86]. Given these observations, one could conclude that even if a Zn(II) MRI CA has a relatively high K_{DZnCA} (i.e., weaker Zn binding) (Fig. 6), it might still participate in certain Zn(II) exchange processes. This might be undesirable if Zn(II) is transferred by the CA to the wrong target. This could occur for example if the Zn(II)-CA complex transfers Zn(II) more rapidly to protein X than to the intended functional protein or enzyme simply based on more favorable molecular interactions between the Zn(II)-CA complex and protein X.

2.1.1.3 Zn(II) selectivity: The Zn(II) binding moieties largely used to date in the design of MRI agents (DPA, and DAA) display high binding selectively for Zn(II) over Na^+, K^+, Ca^{2+} and Mg^{2+}, even when the latter ions are present in much higher concentrations *in vivo* compared to Zn(II). However, these Zn(II) binding units bind Cu(II) with even higher affinity ($\log K_{DCuDPA} \sim 2\log K_{DZnDPA}$) [57]. While one can often ignore free Cu(II) for qualitative detection of Zn(II) because it is present at much lower concentrations than Zn(II) *in vivo*, Cu(II) will interfere with any quantitative attempt to measure free Zn(II) levels. The design of a truly Zn(II) specific agent using small Zn(II) ligands remains an elusive goal. The $3d^{10}$ electron configuration of Zn(II) provides no additional ligand-field stabilization energy so no coordination geometry is inherently more stable than another. Thus, to design a ligand that is more selective for Zn(II) over Cu(II), one might choose a ligand coordination geometry that would result in destabilization of the Cu(II) ligand field. An alternative design for Zn(II) selectivity would be one where r_1 changes upon Zn(II) binding not upon Cu(II) binding. An example of such a design is given by Gd-L^1 (Fig.1).

2.1.1.4 Zn(II) Quantification by MRI: Obtaining a quantitative measure of free Zn(II) by use of a single T_1 shortening agent is complicated by the uncertainty of knowing the exact concentration of the agent *in vivo*. Possible solutions to this problem are 1) to inject two different agents consecutively, one agent that responds to the analyte by a change in r_1 and another that does not [92], or 2) inject two different agents simultaneously, one reporting out

changes in r_1 (the responsive agent) and the another changes in r_2 for example (the non-responsive agent) [93]. One successful example of the second approach was to inject of a cocktail of agents, one being a pH-responsive, largely T_1 agent (Gd) while the other a pH non-responsive, largely T_2 agent (Dy) to obtain a map of tissue pH based upon a map of ΔR_1 and ΔR_2^* values. One could envision using a similar approach to quantify labile Zn(II) concentrations *in vivo* by MRI.

2.2 Fluorescence-based optical imaging

While many more fluorescence-based Zn(II) sensors (Fig. 7) have been reported compared to MRI sensors, only a few have been used to detect Zn(II) *in vivo*. Fluorescence probes are attractive for *in vivo* imaging of Zn(II) because they can be used at much lower concentrations than MRI agents. Nevertheless, the major disadvantage of most optical-based sensors is limited tissue penetration so they can be applied only in select situations [47]. Intravital macroscopic imaging techniques are attractive whenever optical endoscopes or other devices can be positioned near the tissue of interest. In one interesting application of a Zn(II)-sensitive fluorescence probe, ZPP1 (entry **11** in Fig. 7), was used to follow the progression of prostate cancer in a transgenic mouse model *in vivo* [94]. A titration of Zn(II) with ZPP1 showed biphasic behavior where the fluorescence intensity reached a peak maximum when the concentration of ZPP1 was half the concentration of total Zn(II), consistent formation of 2:1 complex. Interestingly, the 2:1 complex was more highly fluorescent than the 1:1 complex, so the sensor was unusually sensitive when fully saturated with Zn(II) [89]. This unique behavior allowed the use of ZPP1 to detect decreases in free Zn(II) in prostate known to accompany cancer progression by use of whole-body fluorescence imaging in the TRAMP mouse model (Fig. 8).

Recently, another fluorescent probe was used to monitor Zn(II) release from cultured β cells and intact pancreatic islets after stimulation by high glucose [91]. The ligand ZIMIR, with two dodecyl side-chains (**27** in Fig 7), when presented to cells quickly integrated (~20 min) into the outer cell membrane and only gradually internalized. Binding of Zn(II) to ZIMIR results in intense fluorescence that can easily be followed by confocal imaging. One interesting and important observation made when using this probe in rat pancreatic islets was that β-cells, when exposed to high glucose, do not exocytose Zn(II) homogenously but rather only a subpopulation of clustered β-cells exhibit robust secretion at any given time. These secretory clusters of β-cells were scattered throughout an islet along with other β-cells that show much weaker secretory activity. Also, it was observed that Zn(II) release occurs in both homologous cell-cell contacts (β-β) and heterologous (β-α) cell-cell contacts with Zn(II) release being rare at other sites within clusters of cells. The authors suggested that ZIMIR could potentially be applied to monitor Zn(II) release from pancreatic β-cells *in vivo* once the Zn(II) affinity and aqueous solubility of the probe are optimized. This of course would require positioning an optical sensor device near the pancreas using endoscopic methods.

3. SUMMARY

Zinc is a unique and limiting micronutrient metal that serves numerous critical biological functions. The tissue distribution of this ion is quite variable and its various chemical forms range from free, unbound or weakly bound Zn(II) ions to tightly-bound, non-immunostainable forms (e.g., in enzymes, zinc fingers, metallothienins). The coordination chemistry of biological Zn(II) and the inability of this ion to participate indirectly in biological redox reactions while allowing for both structural and catalytic participation are deemed critical to the multifaceted role of Zn(II) in biology. The current understanding of Zn(II) ion homeostasis is limited but there a rapidly increasing number of reports that describe various chemical species of Zn(II) in healthy and diseased tissues. A few

fluorescence and MRI probes have enjoyed some success in monitoring differences in levels of free Zn(II) in the pancreas, brain, and prostate and newer sensors with different types of Zn(II) binding moieties and responsive behavior will likely continue to appear in the literature. It will be important to develop a toolbox of different Zn(II) sensors for intravital imaging so that one can develop a much clearer picture of Zn(II) homeostasis *in vivo*. The few early MR imaging strategies recently reported present a new avenue to detect and track free Zn(II) stores *in vivo* and increases the probability of non-invasive human imaging of labile Zn(II) *in vivo*. Given the fraction of the world's population affected by diseases involving abnormal Zn(II) homeostasis including diabetes, BPH/prostate and breast cancers, arthritis, and Alzheimer's disease is already large and growing, ever increasingly sophisticated diagnostic imaging methods will attract more and more interest in monitoring Zn(II) levels in tissues. Any development in the field of non-invasive, whole body imaging of Zn(II) that may allow tracking of the free unbound or weakly bound ion in all tissues simultaneously would offer opportunities to correlate those findings with other clinically relevant data.

Acknowledgments

This research was supported in part by Universidad de Guanajuato (DAIP) Grant 000024/10 and SEP Grant UGTO-CA-107 and by grants from the National Institutes of Health USA (DK-058398, RR-02584 and CA-126608) and Robert A. Welch Foundation Grant AT-584.

References

1. Andreini C, Banci L, Bertini I, Rosato A. J Proteome Res. 2006; 5:3173–3178. [PubMed: 17081069]
2. Tomat E, Lippard SJ. Curr Opin Chem Biol. 2010; 14:225–230. [PubMed: 20097117]
3. Kelleher SL, McCormick NH, Velasquez V, Lopez V. Adv Nutr. 2011; 2:101–111. [PubMed: 22332039]
4. Rink L, Gabriel P. P Nutr Soc. 2000; 59:541–552.
5. Mills, CF. Zinc in Human Biology. Springer-Verlag New York, LLC; New York: 1989.
6. Maret W. Biometals. 2009; 22:149–157. [PubMed: 19130267]
7. Hou JC, Min L, Pessin JE. Vitam Horm (San Diego, CA, U S) FIELD Full Journal Title:Vitamins and Hormones (San Diego, CA,United States). 2009; 80:473–506.
8. Costello LC, Franklin RB. J Biol Inorg Chem. 2010
9. Kelleher SL, Seo YA, Lopez V. Genes Nutr. 2009; 4:83–94. [PubMed: 19340474]
10. Munshi A, Babu S, Kaul S, Shafi G, Rajeshwar K, Alladi S, Jyothy A. Methods Find Exp Clin Pharmacol. 2010; 32:433–436. [PubMed: 20852753]
11. Religa D, Strozyk D, Cherny RA, Volitakis I, Haroutunian V, Winblad B, Naslund J, Bush AI. Neurology. 2006; 67:69–75. [PubMed: 16832080]
12. Mocchegiani E, Bertoni-Freddari C, Marcellini F, Malavolta M. Prog Neurobiol. 2005; 75:367–390. [PubMed: 15927345]
13. Frederickson CJ, Moncrieff DW. Biol Signals. 1994; 3:127–139. [PubMed: 7531563]
14. Giblin LJ, Chang CJ, Bentley AF, Frederickson C, Lippard SJ, Frederickson CJ. J Histochem Cytochem. 2006; 54:311–316. [PubMed: 16260591]
15. Frederickson CJ, Koh JY, Bush AI. Nat Rev Neurosci. 2005; 6:449–462. [PubMed: 15891778]
16. Zalewski PD, Millard SH, Forbes IJ, Kapaniris O, Slavotinek A, Betts WH, Ward AD, Lincoln SF, Mahadevan I. J Histochem Cytochem. 1994; 42:877–884. [PubMed: 8014471]
17. Maret W. Exp Gerontol. 2008; 43:363–369. [PubMed: 18171607]
18. Maret W. Antioxid Redox Signal. 2006; 8:1419–1441. [PubMed: 16987000]
19. Hao Q, Maret W. J Alzheimers Dis. 2005; 8:161–170. discussion 209–115. [PubMed: 16308485]
20. Maret W. Journal of biological inorganic chemistry : JBIC : a publication of the Society of Biological Inorganic Chemistry. 2011; 16:1079–1086. [PubMed: 21647775]

21. Krezel A, Maret W. Journal of biological inorganic chemistry : JBIC : a publication of the Society of Biological Inorganic Chemistry. 2008; 13:401–409. [PubMed: 18074158]
22. Krezel A, Maret W. J Am Chem Soc. 2007; 129:10911–10921. [PubMed: 17696343]
23. Meeusen JW, Nowakowski A, Petering DH. Inorg Chem. 2012
24. Jiang LJ, Maret W, Vallee BL. Proc Natl Acad Sci U S A. 1998; 95:3483–3488. [PubMed: 9520392]
25. Maret W, Krezel A. Mol Med. 2007; 13:371–375. [PubMed: 17622324]
26. Krezel A, Maret W. Biochem J. 2007; 402:551–558. [PubMed: 17134375]
27. Krezel A, Hao Q, Maret W. Arch Biochem Biophys. 2007; 463:188–200. [PubMed: 17391643]
28. Krezel A, Maret W. Journal of biological inorganic chemistry : JBIC : a publication of the Society of Biological Inorganic Chemistry. 2006; 11:1049–1062. [PubMed: 16924557]
29. Sprietsma JE. Med Hypotheses. 1999; 53:6–16. [PubMed: 10499817]
30. Krizkova S, Fabrik I, Adam V, Hrabeta J, Eckschlager T, Kizek R. Bratisl Lek Listy. 2009; 110:93–97. [PubMed: 19408840]
31. Lichten LA, Cousins RJ. Annual review of nutrition. 2009; 29:153–176.
32. Hogstrand C, Kille P, Nicholson RI, Taylor KM. Trends Mol Med. 2009; 15:101–111. [PubMed: 19246244]
33. Hirano, T.; Murakami, M.; Fukada, T.; Nishida, K.; Yamasaki, S.; Suzuki, T. Roles of Zinc and Zinc Signaling in Immunity: Zinc as an Intracellular Signaling Molecule. In: Frederick, WA., editor. Advances in Immunology. Academic Press; 2008. p. 149-176.
34. Eide DJ. Biochim Biophys Acta. 2006; 1763:711–722. [PubMed: 16675045]
35. Bozym RA, Chimienti F, Giblin LJ, Gross GW, Korichneva I, Li Y, Libert S, Maret W, Parviz M, Frederickson CJ, Thompson RB. Exp Biol Med (Maywood). 2010; 235:741–750. [PubMed: 20511678]
36. Eide DJ. Metallomics. 2011; 3:1124–1129. [PubMed: 21789324]
37. Oyama TM, Oyama K, Oyama TB, Ishida S, Okano Y, Oyama Y. Toxicol In Vitro. 2010; 24:737–744. [PubMed: 20079827]
38. Organisciak D, Wong P, Rapp C, Darrow R, Ziesel A, Rangarajan R, Lang J. Photochem Photobiol. 2012
39. Zhao Y, Tan Y, Dai J, Li B, Guo L, Cui J, Wang G, Shi X, Zhang X, Mellen N, Li W, Cai L. Toxicol Lett. 2011; 200:100–106. [PubMed: 21078376]
40. Wijesekara N, Chimienti F, Wheeler MB. Diabetes, Obes Metab. 2009; 11:202–214. [PubMed: 19817803]
41. Song Y, Wang J, Li X-k, Cai L. Biometals. 2005; 18:325–332. [PubMed: 16158224]
42. Pillonetto G, Caumo A, Cobelli C. Am J Physiol Endocrinol Metab. 2010; 298:E440–448. [PubMed: 19920215]
43. Perez-Maraver M, Caballero-Corchuelo J, Boltana A, Insa R, Soler J, Montanya E. Acta Diabetol. 2011
44. Sondergaard LG, Stoltenberg M, Flyvbjerg A, Brock B, Schmitz O, Danscher G, Rungby J. Apmis. 2003; 111:1147–1154. [PubMed: 14678025]
45. Frederickson CJ, Giblin LJ, Krezel A, McAdoo DJ, Mueller RN, Zeng Y, Balaji RV, Masalha R, Thompson RB, Fierke CA, Sarvey JM, de Valdenebro M, Prough DS, Zornow MH. Exp Neurol. 2006; 198:285–293. [PubMed: 16443223]
46. Thompson RB, Peterson D, Mahoney W, Cramer M, Maliwal BP, Suh SW, Frederickson C, Fierke C, Herman P. J Neurosci Methods. 2002; 118:63–75. [PubMed: 12191759]
47. Weissleder R, Pittet MJ. Nature. 2008; 452:580–589. [PubMed: 18385732]
48. Lim NC, Freake HC, Brückner C. Chem Eur J. 2005; 11:38–49. [PubMed: 15484196]
49. Tomat E, Lippard SJ. Current Opinion in Chemical Biology. 2010; 14:225–230. [PubMed: 20097117]
50. Xu Z, Yoon J, Spring DR. Chem Soc Rev. 2010; 39:1996–2006. [PubMed: 20428518]
51. Que EL, Chang CJ. Chem Soc Rev. 2010; 39:51–60. [PubMed: 20023836]
52. Bonnet CS, Tóth E. Future Med Chem. 2010; 2:367–384. [PubMed: 21426172]

53. Dong D, Jing X, Zhang X, Hu X, Wu Y, Duan C. Tetrahedron. 2012; 68:306–310.
54. Mishra A, Logothetis NK, Parker D. Chem Eur J. 2011; 17:1529–1537. [PubMed: 21268155]
55. De Leon-Rodriguez LM, Lubag AJM, Lopez JA, Andreu-de-Riquer G, Alvarado-Monzon JC, Sherry AD. Med Chem Comm. 2012; 3:480–483.
56. Kotera N, Tassali N, Léonce E, Boutin C, Berthault P, Brotin T, Dutasta J-P, Delacour L, Traoré T, Buisson D-A, Taran F, Coudert S, Rousseau B. Angew Chem Int Ed. 2012; 51:4100–4103.
57. Kruppa M, König B. Chem Rev. 2006; 106:3520–3560. [PubMed: 16967915]
58. Major JL, Parigi G, Luchinat C, Meade TJ. Proc Natl Acad Sci U S A. 2007; 104:13881–13886. [PubMed: 17724345]
59. Major JL, Boiteau RM, Meade TJ. Inorg Chem. 2008; 47:10788–10795. [PubMed: 18928280]
60. Zhang XA, Lovejoy KS, Jasanoff A, Lippard SJ. Proc Natl Acad Sci USA. 2007; 104:10780–10785. [PubMed: 17578918]
61. Lee T, Zhang Xa, Dhar S, Faas H, Lippard SJ, Jasanoff A. Chem Biol. 2010; 17:665–673. [PubMed: 20609416]
62. Hanaoka K, Kikuchi K, Urano Y, Nagano T. J Chem Soc, Perkin Trans. 2001; 2:1840–1843.
63. Esqueda AC, López JA, Andreu-de-Riquer G, Alvarado-Monzón JC, Ratnakar J, Lubag AJM, Sherry AD, De León-Rodríguez LM. J Am Chem Soc. 2009; 131:11387–11391. [PubMed: 19630391]
64. Lubag AJM, De Leon-Rodriguez LM, Burgess SC, Sherry AD. Proc Natl Acad Sci USA. 2011; 108:18400–18405. [PubMed: 22025712]
65. Gyulkhandanyan AV, Lee SC, Bikopoulos G, Dai F, Wheeler MB. J Biol Chem. 2006; 281:9361–9372. [PubMed: 16407176]
66. Kim BJ, Kim YH, Kim S, Kim JW, Koh JY, Oh SH, Lee MK, Kim KW, Lee MS. Diabetes. 2000; 49:367–372. [PubMed: 10868957]
67. Virostko J, Radhika A, Poffenberger G, Chen Z, Brissova M, Gilchrist J, Coleman B, Gannon M, Jansen ED, Powers AC. Mol Imaging Biol. 2010; 12:42–53. [PubMed: 19548035]
68. De Leon-Rodriguez LM, Lubag AJM, Malloy CR, Martinez GV, Gillies RJ, Sherry AD. Acc Chem Res. 2009; 42:948–957. [PubMed: 19265438]
69. De Leon-Rodriguez LM, Lubag A, Udugamasooriya DG, Proneth B, Brekken RA, Sun X, Kodadek T, Sherry AD. J Amer Chem Soc. 2010; 132:12829–12831. [PubMed: 20795620]
70. Budde T, Minta A, White JA, Kay AR. Neuroscience. 1997; 79:347–358. [PubMed: 9200720]
71. Costello LC, Franklin RB. J Biol Inorg Chem. 2011; 16:3–8. [PubMed: 21140181]
72. Franklin RB, Milon B, Feng P, Costello LC. Front Biosci. 2005; 10:2230–2239. [PubMed: 15970489]
73. Cuajungco MP, Fagét KY. Brain Res Rev. 2003; 41:44–56. [PubMed: 12505647]
74. Kelleher SL, McCormick NH, Velasquez V, Lopez V. Adv Nutr. 2011; 2:101–111. [PubMed: 22332039]
75. Malakoutikhah M, Teixid M, Giralt E. Angew Chem Int Ed. 2011; 50:7998–8014.
76. Poduslo JF, Wengenack TM, Curran GL, Wisniewski T, Sigurdsson EM, Macura SI, Borowski BJ, Jack CR Jr. Neurobiology of Disease. 2002; 11:315–329. [PubMed: 12505424]
77. Sensi SL, Paoletti P, Bush AI, Sekler I. Nature. 2009; 10:780–792.
78. Bozym RA, Chimienti F, Giblin LJ, Gross GW, Korichneva I, Li Y, Libert S, Maret W, Parviz M, Frederickson CJ, Thompson RB. Exp Biol Med. 2010; 235:741–750.
79. Stewart AJ, Blindauer CA, Berezenko S, Sleep D, Sadler PJ. Proc Natl Acad Sci USA. 2003; 100:3701–3706. [PubMed: 12598656]
80. Krężel A, Maret W. J Am Chem Soc. 2007; 129:10911–10921. [PubMed: 17696343]
81. De Lisle RC, Sarras MP Jr, Hidalgo J, Andrews GK. Am J Phisiol. 1996; 271:C1103–C1110.
82. Hanaoka K, Lubag AJM, Castillo-Muzquiz A, Kodadek T, Sherry AD. Magn Reson Imag. 2008; 26:608–617.
83. Banks WA. Curr Pharm Des. 2004; 10:1365–1370. [PubMed: 15134487]
84. Tõugu V, Karafin A, Palumaa P. J Neurochem. 2008; 104:1249–1259. [PubMed: 18289347]
85. Sun H, Li H, Sadler PJ. Chem Rev. 1999; 99:2817–2842. [PubMed: 11749502]

86. Maret W, Li Y. Chem Rev. 2009; 109:4682–4707. [PubMed: 19728700]
87. Nolan EM, Lippard SJ. Acc Chem Res. 2009; 42:193–203. [PubMed: 18989940]
88. Wong BA, Friedle S, Lippard SJ. Inorg Chem. 2009; 48:7009–7011. [PubMed: 19572729]
89. Zhang X, Hayes D, Smith SJ, Friedle S, Lippard SJ. J Am Chem Soc. 2008; 130:15788–15789. [PubMed: 18975868]
90. Komatsu K, Kikuchi K, Kojima H, Urano Y, Nagano T. J Am Chem Soc. 2005; 127:10197–10204. [PubMed: 16028930]
91. Li D, Chen S, Bellomo EA, Tarasov AI, Kaut C, Rutter GA, Li WH. Proc Natl Acad Sci U S A. 2011; 108:21063–21068. [PubMed: 22160693]
92. Garcia-Martin ML, Martinez GV, Raghunand N, Sherry AD, Zhang S, Gillies RJ. Magn Reson Med. 2006; 55:309–315. [PubMed: 16402385]
93. Martinez GV, Zhang X, García-Martín ML, Morse DL, Woods M, Sherry AD, Gillies RJ. NMR Biomed. 2011; 24:1380–1391. [PubMed: 21604311]
94. Ghosh SK, Kim P, Zhang XA, Yun SH, Moore A, Lippard SJ, Medarova Z. Cancer Res. 2010; 70:6119–6127. [PubMed: 20610630]

Biographies

A. Dean Sherry completed a PhD in Inorganic Chemistry at Kansas State University and was a NIH Postdoctoral Fellow before joining the chemistry faculty at UT-Dallas in 1972. He served as Chair of Chemistry from 1979–90. In 1990, he joined UT Southwestern to work on development of ^{13}C tracers and NMR to study intermediary metabolism in cells, isolated organs, animals and humans and continue his work on responsive MRI contrast agents. He currently holds a Cecil & Ida Green Distinguished Chair in Systems Biology and serves as Director of the newly established Advanced Imaging Research Center at UT Southwestern Medical Center.

Angelo Josue M. Lubag, Jr., Ph.D.

Angelo was born in Balanga, Bataan, Philippines and received his BS and MS degrees from the Institute of Chemistry at the University of the Philippines, Los Baños. He was a Senior Research Associate at the Biochemistry and Analytical Services Laboratories of the Institute of Plant Breeding from 1988 to 1991 and an instructor in chemistry from 1991 to 2000 - both at the University of the Philippines. He received his Ph.D. in Chemistry from the University of Texas at Dallas in 2005 with his dissertation research on the pH Imaging of Ischemia in Rat Hearts using GdDOTA-4AmP. He continued his postdoctoral fellowship

research on the development of molecular imaging using MRI at the University of Texas Southwestern Medical Center in the Department of Radiology/Advanced Imaging Research Center. His current research interests are towards the development of targeted, responsive, and multi-modal (MRI, PET) imaging for biomedical applications - with emphasis on zinc detection and pH mapping.

Luis M. De Leon-Rodriguez received his B.S. in Chemistry in 1996 from the University of Guanajuato and his Ph.D. in Chemistry in 2001 from The University of Texas at Dallas. He is currently Professor of Chemistry at the University of Guanajuato, Mexico. His research interests focus on the synthesis of biospecific agents for molecular imaging and peptide based pharmaceuticals.

Highlights

- Tracking the many forms of Zn *in vivo* is of prime importance.
- Deep-tissue labile or “free” aqueous Zn(II) in cells can be imaged *in vivo*, e.g., MRI.
- Rational Zn chelate design must consider K_D, pZn, and the target microenvironment.
- Non-invasive Zn(II) tracking will need expertise in chemistry, biology, and medicine.

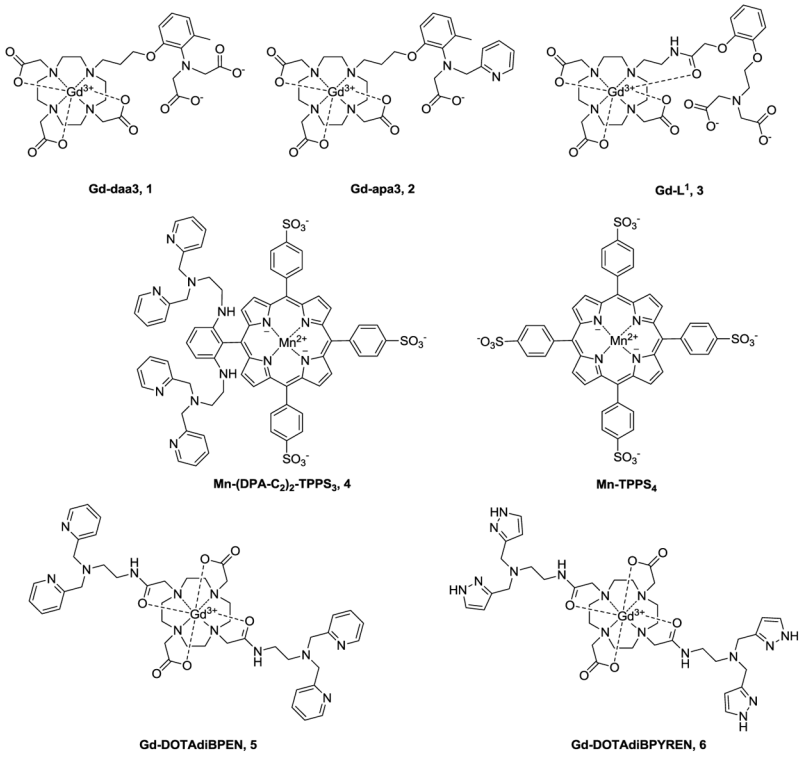

Figure 1.
A few MRI contrast agents that "respond" to the presence of Zn(II).

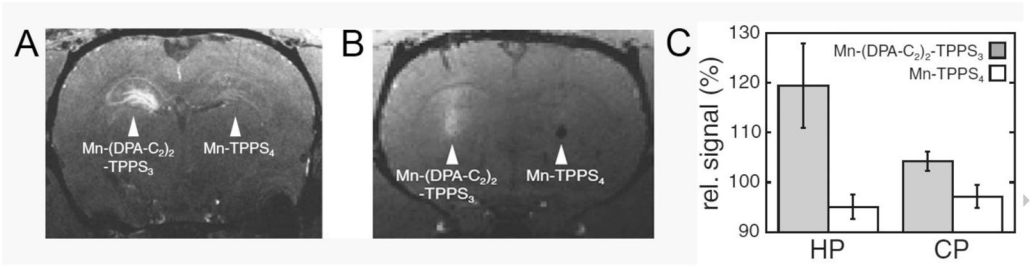

Figure 2.

Contrast enhancement in representative rats, two days after injection of Mn-(DPA-C_2)$_2$-$TPPS_3$ and Mn-$TPPS_4$ into the left and right hemispheres of (A) hippocampus and (B) caudate-putamen. T_1-weighted MRI data were acquired at 9.4 T with (A) 75×75×300 μm voxel size, TE/TR = 6/50 ms, FOV = 30×30×150 mm, and data matrix of 400×400×50 points (4-fold averaging, scan time = 37.3 min) and (B) with 150 μm cubic voxels, TE/TR = 6/50 ms, FOV = 30×30×22.5 mm, and data matrix of 200×200×150 points (no averaging, scan time = 15.5 min). (C) Relative MRI signal quantification in hippocampal (HP) and caudate (CP) regions near the injection sites of Mn-(DPA-C_2)$_2$-$TPPS_3$ (gray) and Mn-$TPPS_4$ (white). Both brain regions show significantly greater contrast enhancement with Mn-(DPA-C_2)$_2$-$TPPS_3$ than with the control compound, but the difference is roughly three times greater on average in the zinc-rich hippocampus than in the caudate, which contains substantially less labile zinc. Error bars denote SEM for n = 6. Reprinted with permission from Elsevier, ref. [61], copyright 2010.

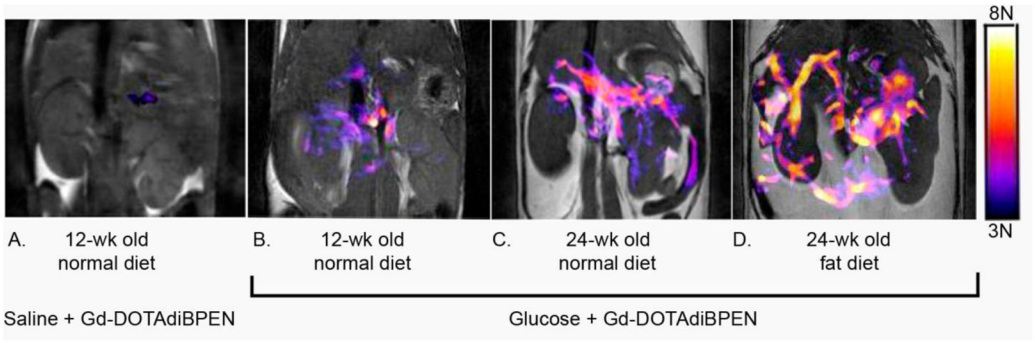

Figure 3.

Representative grayscale T_1-weighted MR images of a single slice through the abdomen that contains a portion of pancreatic tissue (1 mm slice w/o fat saturation) of 12- week old control animal after injection of saline followed by GdDOTA-diBPEN (A) and 12- week old control animal (B), 24-week old mice fed a standard 10% diet (C) or a 60% fat diet (D) over 12 weeks after injection of glucose followed by GdDOTA-diBPEN. The colored overlays represent a 3D composite of those pixels in each of fourteen slices where the water image intensity increased by 3-fold or more over the average noise after injection of saline plus agent or glucose plus agent. From ref. [64] copyright 2011.

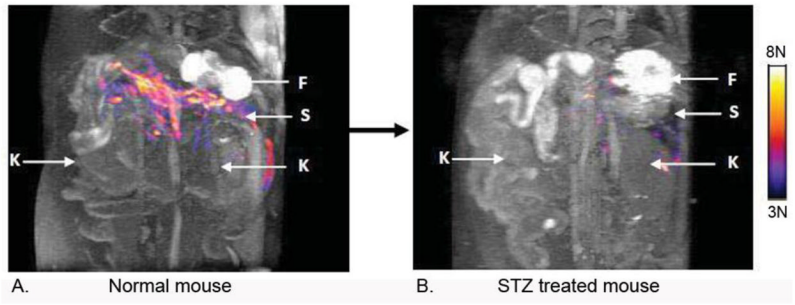

Figure 4.

Images of Zn(II) release during GSIS in a 12 week old control (A) *versus* a STZ-treated mouse (B). The color overlay represents the tissue areas where a contrast enhancement was observed after a bolus injection of GdDOTA-diBPEN and glucose. The colored image overlays reflect the same changes as noted in Fig. 3. The arrows refer to F = fundus stomach, S = spleen, K = kidneys. The images were collected from the same mouse before and 4 days after a single high-dose treatment of STZ. From ref. [64] copyright 2011.

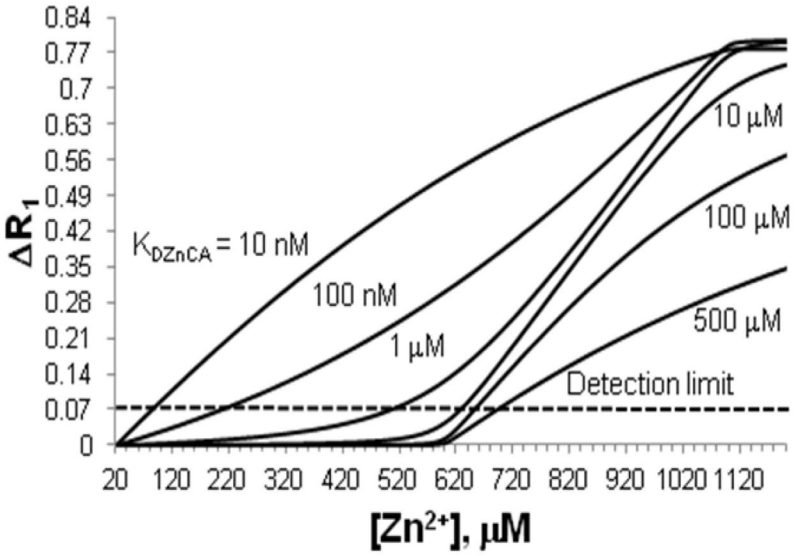

Figure 5.

Calculated plots of ΔR_1 *versus* free Zn(II) levels (plots were calculated using the model defined in [62],[63]). The model assumes HSA = 600 μM, an extracellular concentration of Zn(II) sensor = 50 μM, and a modest increase in r_1 of 40%.

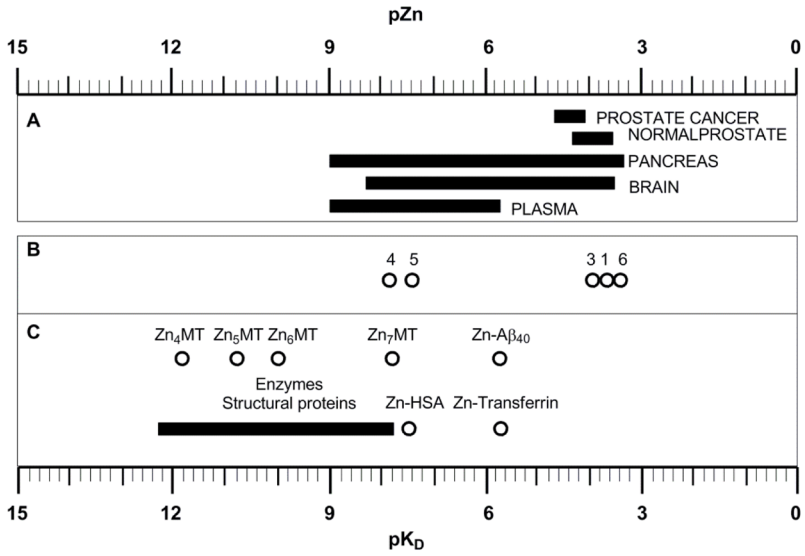

Figure 6.

A) Labile Zn(II) levels in different organs and media; prostate refers to values determined in the cytosol of prostate epithelial cells. B) pK_{DZn} values of the Zn(II) MRI CAs reported in this account. C) pK_{DZn} values of relevant biomolecules. Enzymes and structural proteins and Zn-transferrin pK_D and labile Zn(II) in plasma and prostate cancer were obtained from[6], [17–20], [85], and [72] respectively. Other values were obtained from references cited within the text.

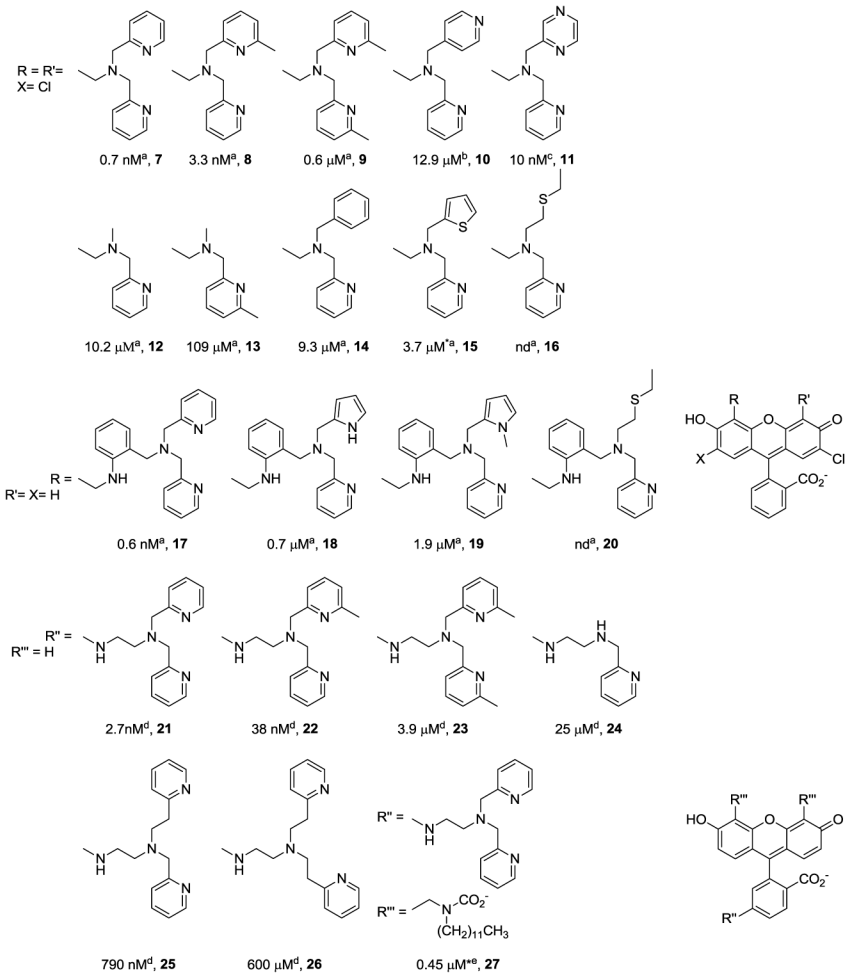

Figure 7.

Zn(II) binding moieties reported for fluorescent sensors. Numbers given below each compound correspond to K_{DZn} values taken from [87][a], [88][b], [89][c], [90][d] and [91][e], * corresponds to a value determined for analog compounds.

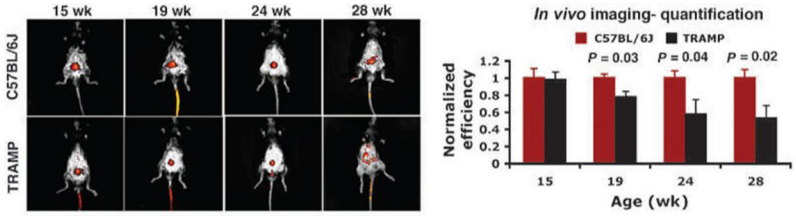

Figure 8.

In vivo detection and monitoring of prostate cancer by epifluorescence whole-body optical imaging. A, noninvasive, whole-body epifluorescence optical imaging of 15-, 19-, 24-, and 28-wk-old TRAMP (bottom) and C57BL/6J (top) mice 30 min after tail-vein injection of ZPP1 (2.5 μmol/Kg if one assumes an average weight of 20 g for a 15 wk old mouse). In TRAMP mice, consistent with prostate cancer progression, there was an overall reduction in prostate-associated fluorescence with age, beginning at 19 wk of age. By contrast, the signal in the C57BL/6J mice remained the same (n = 4). Fluorescence efficiency relative to muscle tissue was normalized to 1. Reprinted by permission from the American Association for Cancer Research: S. K. Ghosh, P. Kim, X. A. Zhang, S. H. Yun, A. Moore, S. J. Lippard, Z. Medarova, A Novel Imaging Approach for Early Detection of Prostate Cancer Based on Endogenous Zinc Sensing, *Cancer Res.* **70**, 6119–6127 (2010); 10.1158/0008-5472.CAN-10-1008.

Table 1

Total Zn content of vesicles, cells or tissues with elevated levels of the metal

ORGAN AND TISSUE/CELLS	Zn LEVEL (total), FORMS	ASSOCIATED DISEASE	REFERENCES
Pancreas			
- β-cells	10–20 mM (*in vesicles*)	Type 1 & Type 2 Diabetes Insulinoma; Pancreatic Ca	[16]
Prostate			
- Epithelial/Ductal (Peripheral)	~ 3 – 4.5 mM (3,000 to 4,500 nmol/g *normal epithelial tissue*) ~ 10 mM (10,000 nmol/g *normal prostatic fluid*) ~ 2.5 mM (*whole prostate*)	Benign Prostatic Hyperplasia (BPH); *Malignant Prostate Cancer* (PCa) : (~400–800 nmol/g = 0.4 mM)	[8] [3]
Breast			
- Mammary cells	(1 – 3 μg Zn excretion/day during lactation)	*Malignant Breast* Cancer (BCa)	[3]
Brain/CNS			
- Neuropil (gray matter)	Control (normal) = 0.346 mM	Alzheimer's = 0.786 mM	[15]
- Plaque (Alzheimer's)	Plaque rim = 1.024 mM Plaque core = 1.327 mM Total senile plaque = 1.055 mM		[15]
Blood (Serum)	12 – 16 μM; (*nM* level)	Hypozincemia (< 10 μM) Hyperzincemia (>20 μM)	[4, 5]

Table 1

Relaxivity and K_{DZn} values of different MRI contrast agents.

CA	B_o, MHz	Conditions, T,Buffer,pH	r_1, mM-1s-1			K_{DZn}
			No Zn(II)	Zn(II)(Cu^{2+})CA:Zn(II)		
Gd-daa3	60	37°C, 100 mM KCl/100 mM Hepes, 7.4	2.3	5.1 (5.1)	1:1	238 μM
	60	37°C, male human serum	5.8	7.7	1:1	ND
Gd-apa3	60	37°C, 100 mM KCl/100 mM Hepes, 7.4	3.4	6.9	1:1	ND
Gd-L[1]	60	37°C, 100 mM MOPS, 7.4	3.7	6.3 (4.5)	1:1	126 μM
	60	37°C, mouse serum	4.0	5.6		316 μM
Mn-(DPA-C_2)$_2$-TPPS$_3$	200	25°C, 25 mM PIPES, 7.0	8.7	6.6	1:1	12 nM
GdDOTA-diBPEN	23	37°C, 100 mM Tris, 7.6	5.0	6.0 (6.3)	1:2	33.6 nM
	400	37°C, 100 mM Tris, 7.6	4.0	4.9		ND
	23	37°C, 100 mM Tris/0.6 mM HSA, 7.6	6.6	17.4 (15.8)		ND
	400	37°C, 100 mM Tris/0.6 mM HSA, 7.6	4.0	6.6		ND
	23	37°C, male human serum	6.1	8.6		ND
GdDOTA-diBPYREN	23	37°C, 100 mM Tris, 7.6	4.2	6.9 (5.5)	1:2	379 μM
	23	37°C, 100 mM Tris/0.6 mM HSA, 7.6	8.4	16.3		ND
	23	37°C, male human serum	6.0	13.1		ND
	400	37°C, 100 mM Tris/0.6 mM HSA, 7.6	3.2	4.0		ND
Prohance™	23	37°C, 100 mM Tris/0.6 mM HSA, 7.6	2.9	2.7		